Hyperspectral Mapping—Combining Cathodoluminescence and X-ray Collection in an Electron Microprobe

COLIN M. MACRAE,[1]* NICHOLAS C. WILSON,[1] SALLY A. JOHNSON,[1] PETER L. PHILLIPS,[1] AND MASAYUKI OTSUKI[2]

[1]*Microbeam Laboratory, CSIRO Minerals, Bayview Avenue, Clayton, Victoria 3168, Australia*
[2]*JEOL Ltd., 1-2 Musashino 3-chome, Akishima, Tokyo 196, Japan*

KEY WORDS cathodoluminescence; electron microprobe; hyperspectral; mapping

ABSTRACT An optical spectrometer has been integrated into a JEOL 8900R electron microprobe, which allows simultaneous collection of light, X-ray, and electron signals. The cathodoluminescence signal is collected from a monocular eyepiece, which is integrated into the electron optics of the electron microprobe. The optical acquisition is synchronized with the stage motion. X-ray lines of major elements are collected using an energy dispersive spectrometer, X-ray lines of minor elements are collected using wavelength dispersive spectrometers, and the secondary and backscattered electron signals are collected using standard detectors. In mapping mode of operation the different signals are collected at each pixel with map sizes typically ranging from 1 million to 10 million pixels. This represents a significant amount of data from which the major correlations and associations in the map can be determined. Summing over a small number of channels and examining only a subset of the complete wavelength range are the strategies that have been developed to reduce the size of the data handled. The application of this mapping technique is demonstrated with two examples, zircons and refractory bricks. Zircons with various degrees of metamictization have been characterized, and inclusions differentiated using a combination of cathodoluminescence and X-ray maps. Examination of refractory bricks reveals subtle chemical changes in the spinel grains. *Microsc. Res. Tech. 67:271–277, 2005.*

INTRODUCTION

When an electron beam interacts with a solid target a number of interactions occur, which produce electrons, X-rays, and photons in the infrared to ultraviolet frequency range. The process of generating the photons is known as cathodoluminescence. In an electron probe microanalyser (EPMA) both the electron and X-ray signals are collected for analysis and imaging. However, apart from viewing emitted light through the optical microscope or video display, it is generally not collected. EPMA may be equipped with an optical spectrometer that can collect all light from within a broad frequency range. Commonly, the optical detector collects all cathodoluminescence frequencies and sums them, and this form of collection is known as panchromatic. If three filters or dichroic mirrors are used to collect three separate frequency bands then these can be displayed as a Red Green Blue (RGB) image (Saijo et al., 2001). If the cathodoluminescence detector is a monochromatic spectrometer then only a single frequency or small range of frequencies can be collected at a time. Although this method can provide useful cathodoluminescence imaging information it is difficult to use such a system in the EPMA, since the optics associated with the monochromator or panchromatic spectrometer must often be moved into place for collection. This then obscures the other detectors (X-ray and backscattered electron) and prevents simultaneous collection.

The EPMA can generate electrons over a wide range of accelerating voltages and maintain a very high current density. The interaction volume of the electron beam with a solid has been modelled by a number of authors (Czyzewski and Joy, 1990; Hovington et al., 1997) and cathodoluminescence resolutions of down to 20 nm have been observed at low voltages (Norman, 2002).

Two strategies for the collection of cathodoluminescence have been developed to deal with the wide range of sample sizes or regions of interest to be examined. For large areas the stage is moved using stepper motors while for small areas the beam is stepped digitally and the cathodoluminescence signal collected during the dwell at each pixel. The largest region over which a beam map of X-rays can be acquired is limited in the EPMA by the distance over which the wavelength dispersive spectrometers maintain focus. This focus is dependent upon the spectrometer position of the element being observed, the d value of the diffracting crystal, and the diameter of the Roland circle. Typically, with single focusing spectrometers they lose focus after 40 μm of beam movement and thus beam maps are not collected greater than this size. The light optics maintains uniform collection efficiency above 100 μm, provided a 400-μm-diameter optical fiber is employed.

We have developed a system in which an optical spectrometer has been integrated into an EPMA, which uses the existing optics for observing reflected

*Correspondence to: Colin MacRae, CSIRO Minerals, Bayview Avenue, Clayton, Victoria 3168, Australia. E-mail: colin.macrae@csiro.au

Received 22 April 2005; accepted in revised form10 June 2005
DOI 10.1002/jemt.20205
Published online in Wiley InterScience (www.interscience.wiley.com).

light images, and allows simultaneous collection of cathodoluminescence, X-ray, and electron signals (MacRae et al., 2001). This form of mapping has significant advantages over traditional mapping in that it removes the need to have a priori knowledge about what the important frequencies are, which will provide the solution to the problem at hand. In addition, a single pass map minimizes the beam dose on the sample and hence the sample damage. Collecting with multiple passes can lead to sample damage, affecting the cathodoluminescence map by increasing or decreasing the observed luminescence.

MATERIALS AND METHODS

System Overview

The cathodoluminescence signal is collected using the existing optic components integrated into a JEOL 8900R SuperProbe. In the electron probe microanalyser (EPMA), a hemispherical mirror collects the light generated at the sample surface and directs it onto a series of mirrors. The light emerges from the microscope as a near parallel beam, and is focused using additional lenses onto an optical fiber that transfers the light to an optical spectrometer. The fiber acts as the entrance slit to the spectrometer and governs the ultimate optical resolution of the spectrometer. Typically, a 200-μm optic fiber is employed with a 300-lines/inch-ruled grating spectrometer, which has a spectral range from 300 to 1,800 nm. This results in an optical resolution of 20 nm. Although the spectrometer collects from 300 to 1,800 nm, the spectral range with a grating efficiency of greater than 30% is 350 to 1,200 nm and generally only the data from the this range is used. Light collected with less than 30% efficiency generally has a signal-to-noise ratio too low to be useful.

The optical spectrometer connects to an analog-to-digital capture card that is mounted on a personal computer bus. The analog-to-digital card has a clock speed of 2 MHz, but in practice the fastest collection and transfer of a single spectrum to the PC is 2 ms. Software overheads associated with data transfer and interpolation reduce the fastest pixel acquisition to 5 ms.

An advantage of the new system is that the spectrometer can be quickly replaced to change the grating and thus employ a different spectral response to measure the cathodoluminescence spectra. For example, when higher resolution between 200 and 850 nm is required a 600-lines/inch-ruled grating spectrometer is employed with an optical resolution of 8 nm. In this configuration a 2048-element linear charge coupled device (CCD) array collects the light. Each pixel on the CCD array is 14 μm wide and 200 μm high, which makes the system relatively sensitive to weak cathodoluminescence signals.

The dark noise from the CCD array can be removed by either a hardware or software method. In the hardware-based technique in our system, no light is exposed to the first 24 channels of the spectrometer and so counts in these channels are attributed to dark noise. The average value of these 24 channels is then subtracted from every other channel, in the acquisition hardware, each time a spectrum is acquired. This strategy has the advantage that it can compensate for a dark noise level that is changing during the acquisition of a map, but assumes that the dark noise in every channel of the CCD is the same as in the first 24. An alternative, software-based technique is to acquire a complete spectrum while the light occluded from the CCD before the map is collected. This dark noise spectrum is then subtracted from each spectrum that is acquired. This approach has the advantage of correcting the dark noise response for each channel in the spectrum but will lead to errors if the dark noise varies because of temperature changes.

The temperature of the spectrometer is regulated by employing a Peltier cooling system to reduce changes in dark noise. This regulates the temperature to $\pm 0.1^{\circ}C$ and reduces dark noise changes due to temperature effects to less than five counts per channel. The temperature regulation is of particular importance when weak cathodoluminescence signals are observed and the background represents a significant proportion of the signal.

Cathodoluminescence and X-ray signals can be mapped in either stage or beam mapping modes. The optic fiber diameter sets the acceptance angle of the light from the collection optics and a 200-μm fiber accepts light over a 10-μm circle, while a 400-μm fiber accepts light over 50 μm. The 400-μm fiber is normally employed for beam mapping as it represents a good compromise between optical resolution and light collection. Optical acquisition is synchronized with either stage movement by monitoring motor pulses used to trigger stage steps or beam movement synchronized by monitoring a beam scan signal. X-ray lines of major and minor elements are collected using either energy-dispersive or wavelength-dispersive spectrometers, and the secondary and backscattered electron signals can be collected in parallel using standard detectors. This technique does not compromise the fast mapping of major or minor elements. Providing the material to be mapped is moderately cathodoluminescence active, the standard mapping conditions (e.g., 15-kV accelerating voltage, 30-nA beam current, and 20-ms dwell time) can be employed to collect cathodoluminescence spectra well above the dark noise background. The integration of the optical spectrometer, computer, and workstation is shown schematically in Figure 1.

Up to 2048 channels of optical data can be collected at each pixel. A single map can contain up to 1024 × 1024 pixels and in addition to the cathodoluminescence data each pixel can also contain X-ray signals from a number of elements and electron signals. Thus a single map can be over 4 GB in size. This represents a significant memory and manipulation problem if the complete data set is analyzed on a PC. To reduce the data loaded into memory a number of cathodoluminescence channels can be combined and typically either 5 or 10 channels are combined and then displayed. This has the added advantage of improving the signal to noise level of the cathodoluminescence signal.

Data Visualization

Maps are displayed on a PC using Chimage (Harrowfield et al., 1993). Elemental X-ray or cathodoluminescence wavelength data can be selected and displayed either as individual sets or as combinations of up to three sets. For example, selecting a wavelength range and displaying this as a single color or grey scale will generate a monochromatic cathodoluminescence map.

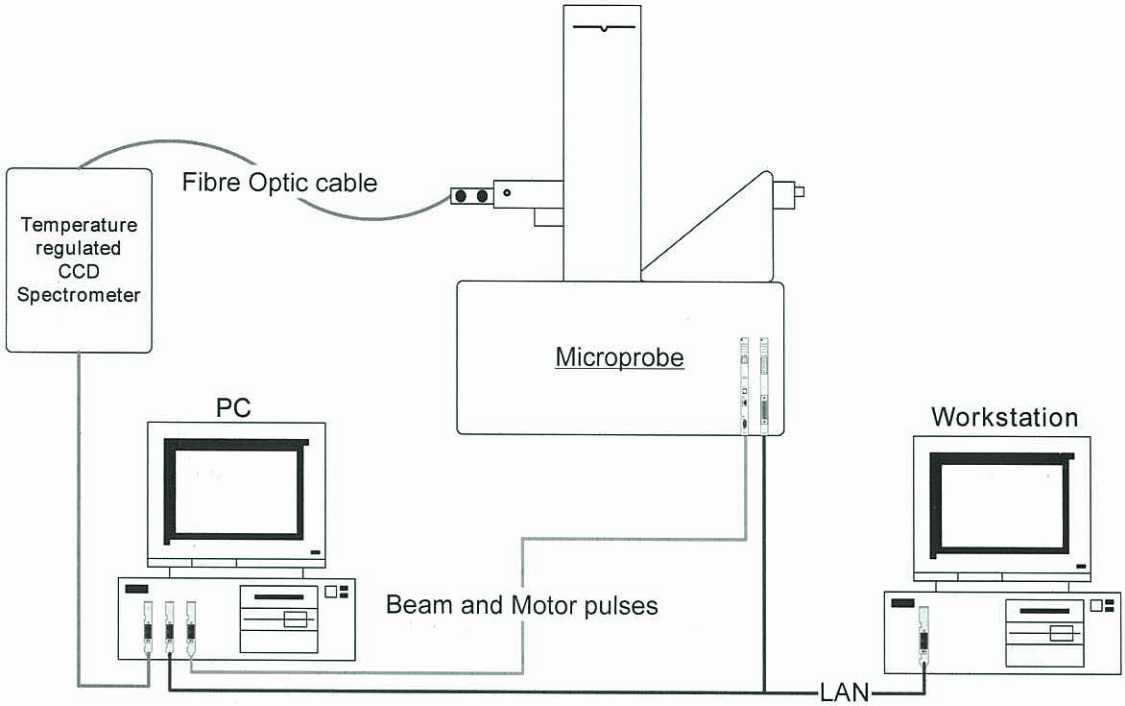

Fig. 1. Schematic drawing of the integrated optical spectrometer, data collection PC, electron microprobe, and associated controlling workstation, which comprise the simultaneous X-ray and cathodoluminescence detection system.

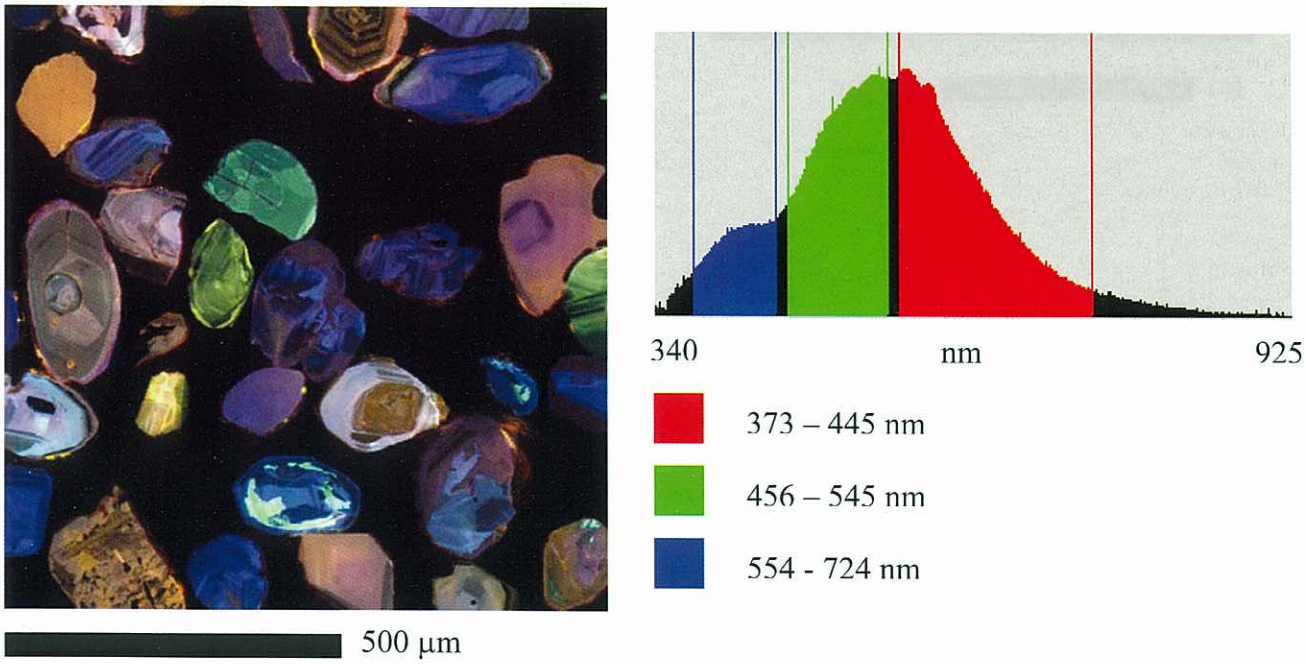

Fig. 2. Three-colour cathodoluminescence map of zircon grains. Three bands are chosen from the summed spectra plot and displayed in the RGB image.

Selecting three discrete wavelengths or bands and displaying them in a map can generate a Red–Green–Blue cathodoluminescence map. Assigning a primary color to each wavelength or element at each pixel generates two- or three-color maps, and the colors are added according to their relative concentrations. An illustration of this method of data visualization using bands is shown in Figure 2, in which three bands of different

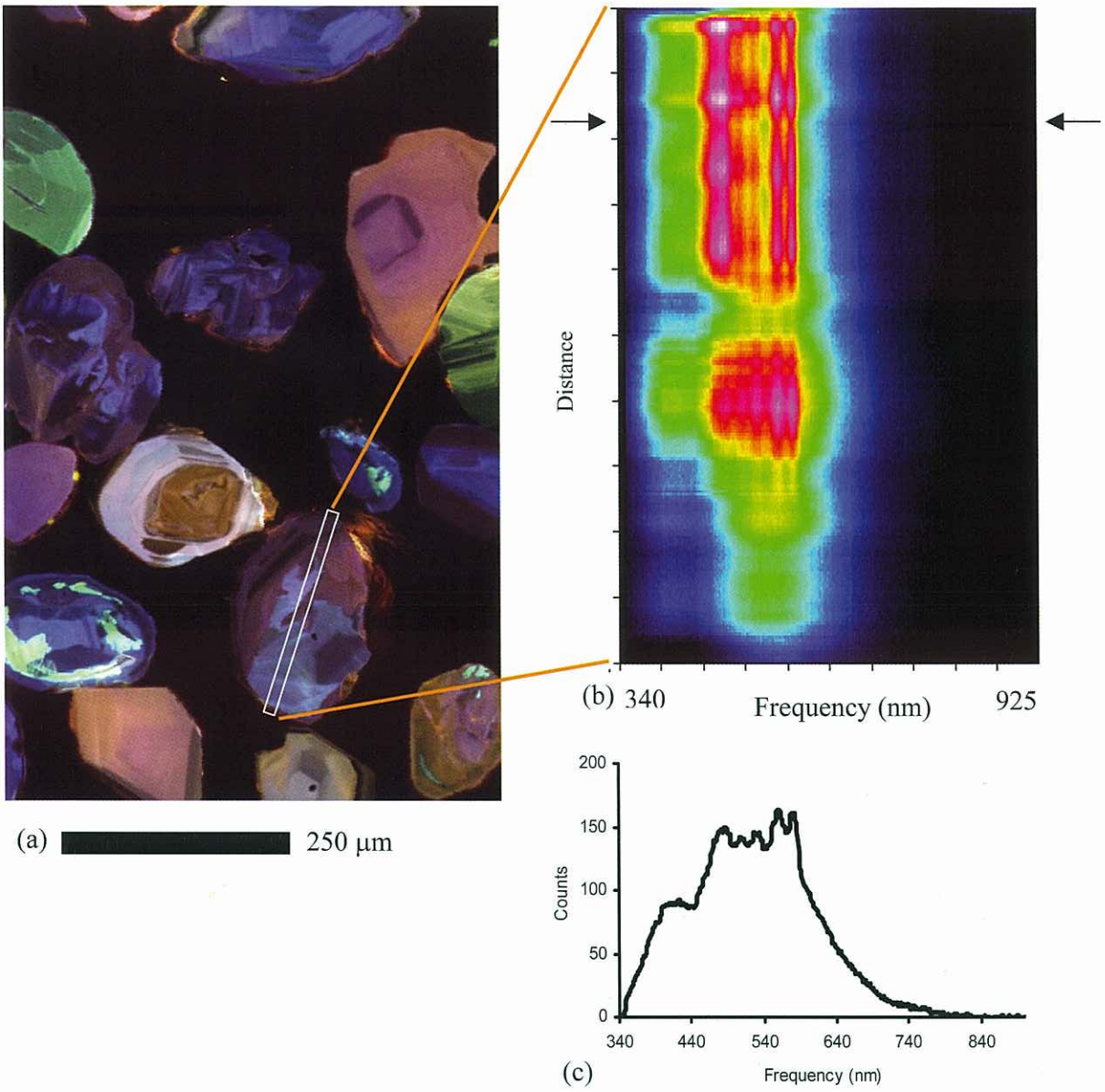

Fig. 3. (**a**) Magnified area of the bottom right of the cathodoluminescence map in figure 2. (**b**) A frequency–distance projection of the marked region shown in (a). Black represents zero counts, with increasing counts represented by blue, green, yellow, red, and white. (**c**) A cathodoluminescence spectra at the position indicated by the arrows on (b).

width have been selected from a summed spectra plot. The summed spectra plot is the average of all spectra in the map. Dominant spectral features are retained in the summed spectra plot, allowing them to be selected as bands. To view minor spectral features, one of two approaches can be taken; (a) spectra from selected areas can be viewed and the presence of minor spectral features examined, or, (b) a frequency–distance projection of a specific line of region can be displayed. This latter approach is shown in Figure 3. This visualization technique can often reveal subtle spectral features that are highly spatially correlated.

The X-ray data within maps is processed prior to display. The elemental peak count-rate recorded at each pixel is divided by the calibrated count-rate taken on a standard of known composition. Collection of the elemental count-rates on a set of standards is part of the routine procedure prior to mapping. The resulting X-ray maps are referred to as *k*-value elemental maps. No correction is made for backgrounds, absorption, or fluorescence of the X-ray within the standard; however, standards are chosen to be as close to the unknown as possible, thus minimizing these problems. If absorption of X-ray lines is significant within a material then each pixel can be post processed through a Bence–Albee matrix correction algorithm incorporated into Chimage. This is especially important when light elements are being mapped.

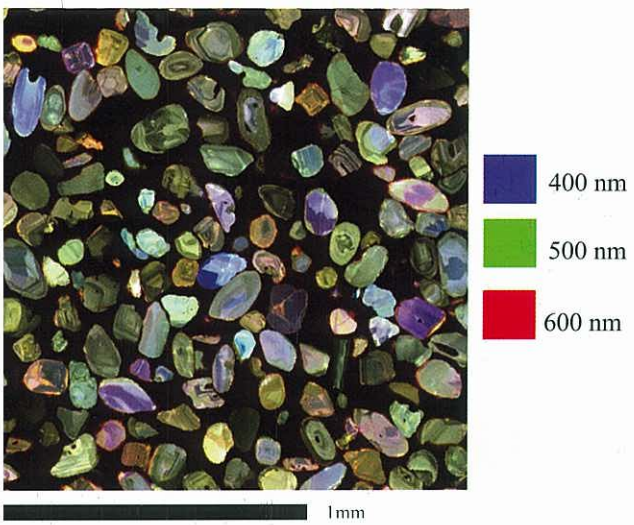

Fig. 4. Zircon grains imaged with cathodoluminescence showing ırious degrees of alteration and metamictization.

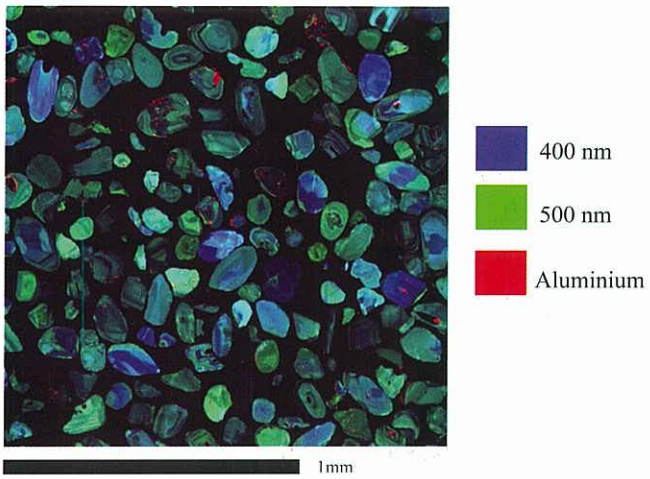

Fig. 5. Zircon grains imaged with cathodoluminescence and Al Kα X-rays showing a number of inclusions and coatings, in red.

Sample Preparation

The types of samples examined in this study were ɔlished sections prepared by mounting in epoxy resin, ıd sectioning and grinding with a final polish of 1-μm ıamond. To remove residual amorphous layers left by ıe diamond polishing, the surfaces were given a fur- ıer finish using 20-nm colloidal silica. Enhanced cath- ɗoluminescence emission and finer structure were ɔserved after this step. The specimens were coated ith a thin conducting layer of carbon prior to irradia- on to prevent deflection of the incident electron beam y charging of the specimen surface. The thickness of ıe carbon coat was estimated to be 15 nm by observing ıterference colors generated on a polished brass sur- ıce coated simultaneously.

RESULTS AND DISCUSSION

Cathodoluminescence microscopy has been applied ı mineral exploration and beneficiation, and the study ' industrial minerals (Götze, 2000; Hagni, 1985, 1986; emond et al., 1992). In this study applications of cath- ɗoluminescence microscopy to zircon grains and alu- ıina–chrome refractory material are presented.

Zircons

Zircons ($ZrSiO_4$) are ubiquitous in the Earth's crust ıd have low solubility in almost all melt and fluid ɔmpositions, allowing them to survive almost any ystal process (Hanchar and Miller, 1993). They con- ıin significant levels of U and Th, which decay radio- ctively to Pb. The diffusion of Pb in zircon is extremely ow and so it retains age information about events ırough subsequent high-temperature fluctuations, ıaking it an extremely important mineral for geochro- ɔlogy. Furthermore, zircons have been extensively ıudied using cathodoluminescence to investigate the ɔrrelation between trace rare earth elements. In par- cular, Dy^{3+} is considered to be the principal spectral ıctor, although other trace constituents such as Sm^{3+}, u^{3+}, Gd^{3+}, Tb^{3+}, and Y^{3+} may also contribute strong lines in the observed emission (Cesbron et al., 1995; Ohnenstetter et al., 1992).

Bangladeshi zircons containing significant levels of thorium and uranium have been investigated using X-rays and cathodoluminescence as illustrated in Figures 4 and 5. In Figure 4, a number of grains have been mapped at 20-kV accelerating voltage, 100-nA beam current and 20 ms/pixel dwell time. Three discrete cathodoluminescence frequencies have been selected and are shown in the cathodoluminescence map. Changes in luminescence are clearly seen, and these are attributed to trace element content, annealing of luminescence centers by radioactive radiation related to U and Th contents, and distortion of band structure in the crystal caused by metamictization (Kempe et al., 2000; MacRae et al., 2003). A number of grains from this deposit contain inclusions of Al silicate that are shown as the red regions in Figure 5. The Al silicate inclusions impart, to some extent, color to the concentrate and reduce its commercial value (Aral, 2000). This image highlights the strength of having a combined X-ray and cathodoluminescence data set. Although this type of information could be obtained separately, the ability to show elemental levels in conjunction with cathodoluminescence allows one to determine whether the cathodoluminescence is due to structural variations or chemical changes. In this case the cathodoluminescence allows one to see growth zones in the zircons, whereas the element information defines the distribution of undesirable impurity elements.

Refractory Materials

Refractory materials are commonly used in high-temperature industrial processes because of their high-temperature mechanical properties. To enhance the time between refurbishments of the refractories, the microstructure of the material should be well understood. Refractory materials are well suited to examination by cathodoluminescence microscopy because a number of the constituent phases exhibit strong cathodoluminescence. For example periclase (MgO), corundum (Al_2O_3), and spinel ($MgAl_2O_4$) structures have all been examined using cathodoluminescence microscopy

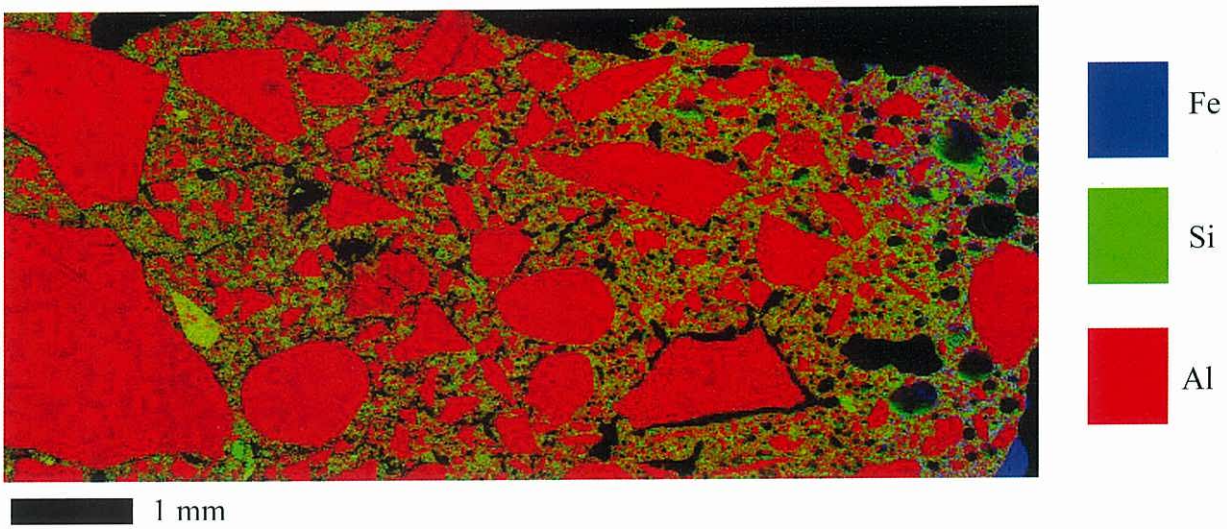

Fig. 6. Elemental maps of an alumina–chrome refractory brick exposed to a number of thermal cycles showing the penetration of Fe from the right-hand side into the brick.

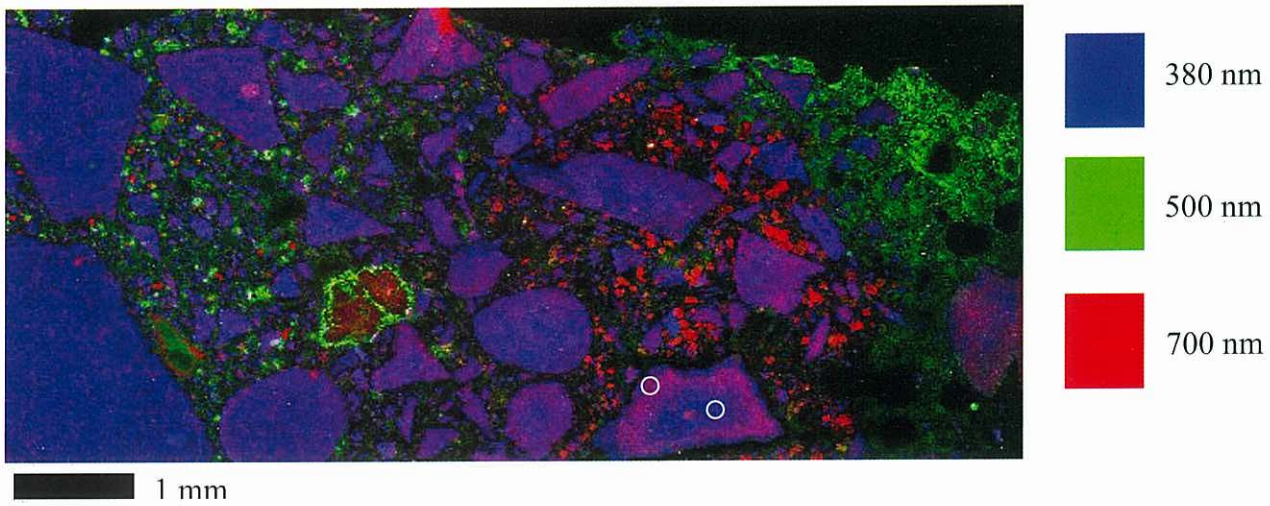

Fig. 7. Three discrete cathodoluminescence frequencies from the map of an alumina–chrome brick described in figure 6. The colour change in the large grains is examined by selecting two areas (highlighted) and examining the spectra.

(Karakus et al., 2000a,b; Vu et al., 1998). The cathodoluminescent-active refractory phases can be quickly detected, their distributions examined, and the extent of elemental substitutions within particular grains can be readily assessed using X-rays. The assessment of both alumina–chrome and chrome-free refractory materials, which are used for line smelting, converting, and refining furnaces, have been studied using optical microscopy, backscattered electron imaging, and cathodoluminescence to determine the depth of penetration of slag into the refractory brick (Karakus et al., 2000a; Moore and Karakus, 1994). Here we present images collected on an alumina–chrome refractory that has been exposed to a number of thermal temperature cycles and exhibits significant chemical changes across the section investigated. The refractory brick was exposed to Fe and slag in the furnace and elemental changes, including penetration of Fe into the brick, can be observed on the right-hand side of Figure 6. The associated cathodoluminescence map of the alumina–chrome brick Figure 7 reveals subtle changes occurring through a number of the larger grains because of the thermal cycling. Two cathodoluminescence spectra, Figure 8, taken from selected areas on both the core and rim of the grain indicated in Figure 7 show different spectral responses. On first inspection, the X-ray maps do not show any difference between core and rim. However, by selecting areas on the core and rim, and averaging the X-ray data from the pixels in each area, a difference in Mg concentration is observed between the core and rim. The Mg concentration in the rim is of order of 200 ppm higher than that in the core. This illustrates the sensitivity of the cathodoluminescence signal to trace element variations and the importance of having a combined X-ray and cathodoluminescence data set.

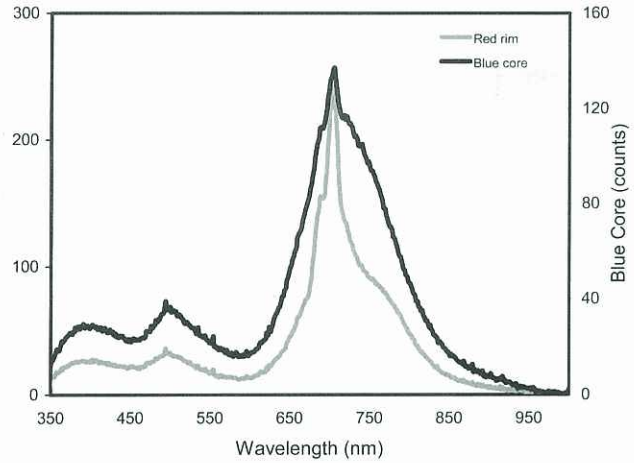

Fig. 8. Selected area cathodoluminescence spectra taken from the re and rim of the grain in Figure 7. The difference in the spectra n be related to various Mg concentrations across the grain.

CONCLUSIONS

A cathodoluminescence detection system with 2048 ıannels has been incorporated into an electron icroprobe, with the ability to simultaneously collect aps of electron signals, X-rays, and cathodolumines- ıce which facilitates the examination of cathodolu- inescence activate materials. This system has been plied to the characterization of zircons, in which the ructure within the zircon grains is important for geo- ıronology. Various degrees of metamictization are early seen in the cathodoluminescence signal, and clusions of aluminum silicates are revealed in the Al -ray map.

An alumina–chrome refractory brick has been exam- ed, and the cathodoluminescence signal has revealed ıbtle changes in wavelength and intensity between re and rims within some aluminum oxide grains. The ssociated X-ray signals have revealed that these ıbtle changes are due to various Mg concentrations.

The ability of the cathodoluminescence signal to veal subtle chemical and structural changes means at this technique of combined electron, X-ray, and hole spectrum cathodoluminescence mapping should ıd applications in the analysis of a wide range of icroanalysis problems.

ACKNOWLEDGMENTS

The authors thank Cameron Davidson for his help in eparing all the sections examined in this study and r. Mark Pownceby for his critical reading of the anuscript.

REFERENCES

Aral H. 2000. Impurities in a Murray Basin zircon sand. International Congress on Mineral Processing and Extractive Metallurgy, MINPREX 2000, Melbourne. 373–379.

Cesbron F, Blanc P, Ohnenstetter D, Remond G. 1995. Cathodoluminescence of rare earth doped zircons. I. Their possible use as reference materials. Scanning Microsc Suppl 9:35–36.

Czyzewski Z, Joy DC. 1990. Monte-Carlo simulation of CL and EBIC contrasts for isolated dislocations. Scanning 12:5–12.

Götze J. 2000. Materials characterisation by cathodoluminescence microscopy and spectroscopy. In: Proceedings of the Sixth International Congress on Applied Mineralogy in Research, Economy, Technology, Ecology and Culture. 783–786.

Hagni RD. 1985. Cathodoluminescence microscopy applied to mineral exploration and beneficiation. In: Proceedings of the Second International Congress on Applied Mineralogy in the Minerals Industry. 41–66.

Hagni RD. 1986. Industrial applications of cathodoluminescence microscopy. Process mineralogy VI. Warrendale, PA: TMS. pp. 37–52.

Hanchar JM, Miller CF. 1993. Zircon zonation patterns as revealed by cathodoluminescence and backscattered electron images: implications for interpretation of complex crystal histories. Chem Geol 110:1–13.

Harrowfield IR, MacRae C, Wilson NC. 1993. Chemical imaging in electron microprobes. In: Proceedings of the 27th Annual Microbeam Analysis Society (MAS) Meeting. 547–548.

Hovington P, Drouin D, Gauvin R. 1997. Casino: a new Monte Carlo code in C language for electron beam interaction. 1. Description of the program. Scanning 19:1–14.

Karakus M, Crites MD, Schlesinger ME. 2000a. Cathodoluminescence microscopy characterization of chrome-free refractories for copper smelting and converting furnaces. J Microsc 200:50–58.

Karakus M, Smith JD, Moore RE. 2000b. Cathodoluminescence mineralogy of used MgO-C bricks in basic oxygen furnaces. Veitsch-Radex Rundschau. 24–32.

Kempe U, Gruner T, Nasdala L, Wolf D. 2000. Relevance of cathodoluminescence for the interpretation of U-Pb zircon ages, with an example of an application to a study of zircons from the Saxonian Granulite Complex, Germany. In: Pagel M, Barbin V, Blanc P, Ohnenstetter D, editors. Cathodoluminescence in Geosciences. Germany: Springer-Verlag. pp. 415–455.

MacRae CM, Wilson NC, Otsuki M. 2001. Holistic mapping. AMAS VI–The Sixth Biennial Symposium in conjunction with SPM III—The Third Scanned Probe Microscopy Conference. 68–69.

MacRae CM, Wilson NC, Aral H, Ryan CG, Pownceby MI. 2003. Zircon characterisation—a new approach to an age old problem. In: Heavy Minerals Conference 2003. 139–143.

Moore RE, Karakus M. 1994. Cathodoluminescence microscopy: a technique uniquely suited to the solution of refractory wear problems. In: Proceedings of the International Ceramics Conference, Austceram 94. 1:925–940.

Norman CE. 2002. Reaching the spatial resolution limits of SEM-based CL and EBIC. Microsc Analy 26:5–8.

Ohnenstetter D, Cesbron F, Remond G, Caruba R, Claude JM. 1992. Émissions de cathodoluminescence de deux populations de zircons naturels: tentative d'interprétation. Comptes Rendus de l'Académie des Sciences, series II. 313:641–647.

Remond G, Cesborn F, Chapoulie R, Ohnenstetter D, Roques-Carmes C, Schvoerer M. 1992. Cathodoluminescence applied to the microcharacterization on mineral materials: a present status in experimentation and interpretation. Scanning Microsc 6:23–68.

Saijo H, Isshiki T, Shiojiri M. 2001. Multi-band cathodoluminescence microscopy for materials science. Solid State Phenomena.78–79:133–138.

Vu TA, Götze J, Burkhardt J, Ulbricht J, Habermann D. 1998. Application of optical and spectral cathodoluminescence in the study of MgO refractories. Interceram 47:164–167.